The anti-toxin ParD of plasmid RK2 consists of two structurally distinct moieties and belongs to the ribbon-helix-helix family of DNA-binding proteins

Monika OBERER*, Klaus ZANGGER†, Stefan PRYTULLA‡ and Walter KELLER*[1]

*Institut für Chemie, Arbeitsgruppe Strukturbiologie, Karl-Franzens-Universität Graz, Heinrichstrasse 28, A-8010 Graz, Austria, †Institut für Chemie, Bereich Organische Chemie, Karl-Franzens-Universität Graz, Heinrichstrasse 28, A-8010 Graz, Austria, and ‡m-phasys GmbH, Vor dem Kreuzberg 17, D-72070 Tübingen, Germany

NMR and CD spectroscopy have been used to characterize, both structurally and dynamically, the 82-amino-acid ParD protein of the post-segregational killing module of the broad-host-range plasmid RP4/RK2. ParD occurs as a dimer in solution and exercises two different control functions; an autoregulatory function by binding to its own promoter P_{parDE} and a plasmid-stabilizing function by inhibiting ParE toxicity in cells that express ParD and ParE. Analysis of the secondary structure based on the chemical-shift indices, sequential nuclear Overhauser enhancements (NOEs) and $^3J_{H\alpha\text{-}NH}$ scalar coupling constants showed that the N-terminal domain of ParD consists of a short β-ribbon followed by three α-helices, demonstrating that ParD contains a ribbon-helix-helix fold, a DNA-binding motif found in a family of small prokaryotic repressors. ^{15}N longitudinal (T_1) and transverse (T_2) relaxation measurements and heteronuclear NOEs showed that ParD is divided into two separate domains, a well-ordered N-terminal domain and a very flexible C-terminal domain. An increase in secondary structure was observed upon addition of trifluoroethanol, suggested to result from the formation of structured stretches in the C-terminal part of the protein. This is the first experimental evidence that the DNA-binding domain of ParD belongs to the ribbon-helix-helix fold family, and this structural motif is proposed to be present in functionally similar antidote proteins.

Key words: autoregulation, CD, NMR, plasmid-addiction system, relaxation.

INTRODUCTION

Plasmid-addiction systems are genetic entities of low-copy-number plasmids (for reviews, see [1–6]) that selectively kill plasmid-free cells and thus mediate stable inheritance of the plasmid in bacteria. They consist of an operon coding for two small proteins, acting as a toxin and an anti-toxin. The comparatively less stable anti-toxin counteracts toxicity by forming a toxin–antidote complex and exhibits negative autoregulatory activity through DNA binding to its promoter region. Plasmid-cured cells cannot produce the antidote, leaving the stable toxin uncomplexed, which consequently causes cell killing or growth retardation [7]. The *parDE* operon of broad-host-range plasmid RP4/RK2 constitutes such a plasmid-addiction system and has been characterized in terms of genetics and function [8,9], together with other killing modules of extrachromosomal elements. Recent studies include *ccd* of plasmid F [10], *parD* and *pem* of plasmids R1 and R100 [11], *phd*/*doc* of prophage P1 [12] and *pas* of plasmid pTF-FC2 [4].

Homologous host-addiction gene systems have also been found on the linear plasmid pCLP from the opportunistic pathogen *Mycobacterium celatum* [13] and on the chromosomes of *Escherichia coli* [14], the human pathogen *Vibrio cholerae* [15] and the plant pathogen *Xylella fastidiosa* [16]. It has been suggested that chromosomally encoded addiction systems are responsible for programmed cell death under conditions of environmental or nutritional stress [3].

ParD exhibits two functions: (i) inhibition or reversal of the toxic effect of ParE and (ii) regulation of the *parDE* operon. The first task is accomplished by building a ParD–ParE complex, whereas the regulatory function results from ParD binding to a site in its own promoter region. A repression-defective mutant of ParD showing an insertion in the N-terminal region of ParD was isolated. This mutant had lost its DNA binding [17], but still exhibited anti-toxic activity, suggesting that the ParD protein is composed of two separate functional regions. A similar distribution of functional domains has been suggested for the CcdA protein [18] and other anti-toxins of plasmid-addiction systems. To date, no three-dimensional (3D) structural information is available for any of these anti-toxins. Previously we have shown that ParD exists as a dimer in solution (18 kDa) and binds to double-stranded oligonucleotides containing the native binding site [8]. Here we report experimental evidence that the proposed two-domain structure of ParD consists of a well-structured N-terminal domain and a relatively unstructured C-terminal domain, and for its classification as a member of the ribbon-helix-helix DNA-binding protein family, similar to the prokaryotic transcriptional repressors Arc, MetJ, Mnt and CopG [19,20], based on the complete assignments of ^{1}H, ^{15}N and ^{13}C resonances and backbone-relaxation data. These data provide the basis for determining the 3D structure of the ParD protein and for understanding its dual role in plasmid stabilization.

EXPERIMENTAL

Protein expression and purification

The uniformly ^{15}N- and ^{13}C-labelled ParD protein was expressed and purified using a slightly modified version of the procedure described in [8], in order to avoid proteolytic degradation. In

Abbreviations used: NOE, nuclear Overhauser enhancement; HSQC, heteronuclear single quantum coherence; CSI, chemical-shift index; TFE, 2,2,2-trifluoroethanol; MALDI–TOF MS, matrix-assisted laser-desorption ionization–time-of-flight MS; 2D, two-dimensional; 3D, three-dimensional.

[1] To whom correspondence should be addressed (e-mail walter.keller@uni-graz.at).

brief, the induced cells were harvested, lysed by sonication and after centrifugation the soluble fraction was heated to 85–90 °C for 3–5 min. After slowly cooling to room temperature and centrifugation the degraded impurities remained in the insoluble pellet, whereas refolded ParD remained in the soluble supernatant and was purified according to the described protocol [8], comprising a heparin column chromatography step followed by anion-exchange and size-exclusion chromatography. Uniformly labelled samples were produced in minimal medium (6.8 g/l Na_2HPO_4/3.0 g/l KH_2PO_4/0.5 g/l NaCl) containing 1.5 g/l $(^{15}NH_4)_2SO_4$ and 2.0 g/l [^{13}C]glucose as the sole nitrogen and carbon sources, respectively. The medium was complemented with 1 μg/l biotin, 1 μg/l thiamin and 1 ml of 1000 × microsalts [1 M $MgCl_2$/150 mM $CaCl_2$/20 mM $FeCl_3$/50 mM H_3BO_3/150 μM $CoCl_2$/800 μM $CuCl_2$/1 mM $MnCl_2$/1.5 mM $ZnCl_2$/15 μM $(NH_4)_6$-Mo_7O_{24},4H_2O].

The molecular mass of the protein was determined by matrix-assisted laser-desorption ionization–time-of-flight MS (MALDI–TOF MS) on a Shimadzu Kompakt MALDI II mass spectrometer. ParD (0.4 mg/ml) was applied to a reversed-phase HPLC column and eluted with an acetonitrile gradient and 0.1 % trifluoracetic acid. α-Cyano-4-hydroxy-cinnamic acid was used as the matrix.

The NMR samples contained about 0.6 mM ParD protein based on the molecular mass of monomeric ParD in 90 % buffer (20 mM phosphate, pH 6.0/50 mM KCl) and 10 % ^2H_2O.

NMR spectroscopy

All NMR measurements were performed at 30 °C on a Varian Unity INOVA 600 MHz spectrometer equipped with a triple-resonance z-gradient probe. The assignment of ^{1}H, ^{15}N and ^{13}C resonances was based on the following experiments: two-dimensional (2D) ^{1}H-^{15}N-heteronuclear single quantum coherence (HSQC), 2D TOCSY, 3D HNCACB, 3D CBCA(CO)NH, 3D HNCO, 3D HN(CA)CO, ^{15}N-edited TOCSY-HSQC and 3D HCCH-TOCSY (for a review, see [21]). The correctness of the NMR backbone assignments was confirmed by sequential nuclear Overhauser enhancements (NOEs) in the ^{15}N-edited NOESY-HSQC spectra. The ^{1}H chemical shifts were calibrated relative to 2,2-dimethyl-2-silapentane-5-sulphonate, sodium salt; ^{15}N and ^{13}C shifts were indirectly referenced [21]. The data were processed using NMRPipe software [22], and visualized and analysed with the XEASY program suite [23] as well as NMRView [24]. $^3J_{\alpha H\text{-}NH}$ coupling constants were calculated from the integrated peaks of an HNHA experiment. ^{15}N longitudinal (T_1) and transverse (T_2) relaxation times were obtained by measuring peak heights and using the two-parameter fit $I(t) = I_0 \exp(-t/T)$. The [^{1}H]-^{15}N-heteronuclear NOEs were obtained from the ratio of peak intensity for ^{1}H-saturated and -unsaturated spectra (saturation time, 2.5 s). Slowly exchanging NH protons were detected by recording two ^{1}H-^{15}N-HSQC spectra after dissolution of lyophilized ^{15}N-labelled ParD protein (20 mM phosphate, pH 6.0/50 mM KCl) in ^2H_2O after 45 and 120 min.

Structure prediction and sequence alignments

A multiple sequence alignment of ParD, other known members of the ribbon-helix-helix family of proteins and the antidote PasA [25] was generated using CLUSTAL W (version 1.8, June 1999) [26] with the following parameters: weight matrix, blosum; gap-opening penalty, 15; gap-extension penalty, 0.05; hydrophilic gaps and residue-specific gap penalties, on; hydrophilic residues, GPSDQERK. In addition, secondary-structure predictions and database threading were performed using the programs PSIPred [27] and GenTHREADER [28]. GenTHREADER yielded an alignment of the N-terminal part of ParD (Met^1–Lys^{50}) with CopG protein (PDB code, 2cpg [29]). This alignment, however, contained a 3-amino-acid gap inserted between helices A and B. Closing this gap resulted in an intact short turn and conserved hydrophobic positions in helix B, in agreement with the multiple alignment.

Conformational changes under hydrophobic conditions

The influence of 2,2,2-trifluoroethanol (TFE) was monitored by titrating TFE into the ^{15}N-labelled sample to reach final concentrations of 1, 3, 5, 10 and 15 % TFE. The normalized shift differences were calculated for each residue that could be unambiguously identified using the equation:

$$\mathrm{norm}\Delta\delta = \Delta\delta|^1\mathrm{H}| + 0.2 \cdot \Delta\delta|^{15}\mathrm{N}|$$

where $\Delta\delta|^1$H| and $\Delta\delta|^{15}$N| are the absolute values of the chemical-shift differences of amide protons and nitrogen atoms, respectively. Unlabelled ParD protein at a final concentration of 23 μM, in 20 mM potassium phosphate buffer, pH 7.5/20 mM KCl, incubated with increasing amounts of TFE (0–80 %), was used for CD measurements carried out on a Jasco J-715 spectropolarimeter. Five averages were taken for each spectrum with the following parameters: step resolution, 0.2 nm; speed, 50 nm/min; response, 1 s; bandwidth, 1.0 nm. The secondary-structure contents were estimated using the secondary-structure estimation program provided by Jasco.

RESULTS

Protein purification

Expression and purification of labelled and unlabelled ParD were performed essentially as described in [8] except that a heat-denaturation and refolding step was introduced prior to the first chromatography step. It has been shown previously by gel-shift analysis [17], CD spectroscopy and differential scanning calorimetry [8] that ParD regains its DNA-binding activity and its native fold after heat treatment. The existence of the dimeric form of ParD was verified using glutaraldehyde cross-linking and gel-permeation chromatography (results not shown). The susceptibility to proteolytic degradation formed a serious obstacle to NMR spectroscopic investigations because data had to be collected with several preparations of ParD and the integrity of the protein had to be checked frequently by recording ^{15}N-HSQC spectra. The initial experiments for the assignment of the backbone were carried out with ParD purified according to the established protocol. All subsequently performed NMR spectra were obtained with heat-treated ParD, which exhibited stability and intactness even over extended measurement times. The agreement of the chemical shifts between both sets of experiments indicated clearly that the native fold of ParD was recovered after heat treatment.

The integrity and uniform labelling of ParD protein were confirmed by MALDI–TOF MS (Figure 1). The experimentally obtained molecular mass of 9467 Da corresponds to a fully ^{13}C- and ^{15}N-labelled protein devoid of Met^1. The theoretical molecular mass was 9470 Da.

Resonance assignment and structural features

For ParD protein, 79 out of 80 possible backbone amide resonances (83 residues minus Pro^{37}, the missing Met^1 and N-terminal Ser^2) in the ^{15}N-HSQC spectrum were assigned un-

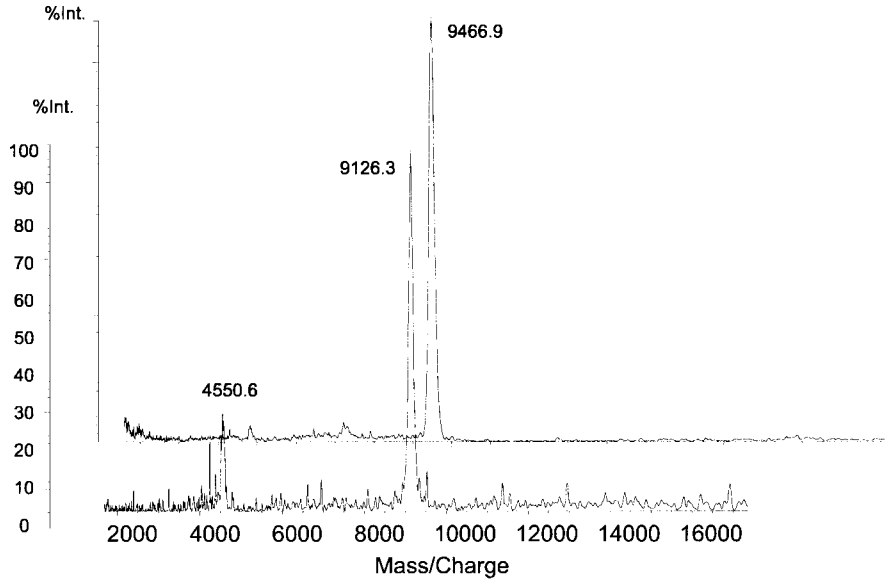

Figure 1 MALDI–TOF spectra of unlabelled and ^{13}C- and ^{15}N-labelled ParD

The mass spectra of purified ParD show the main peaks at $m/z = 9126$ and 9467 Da, corresponding to the integer unlabelled and labelled proteins, respectively. %Int, relative peak intensity.

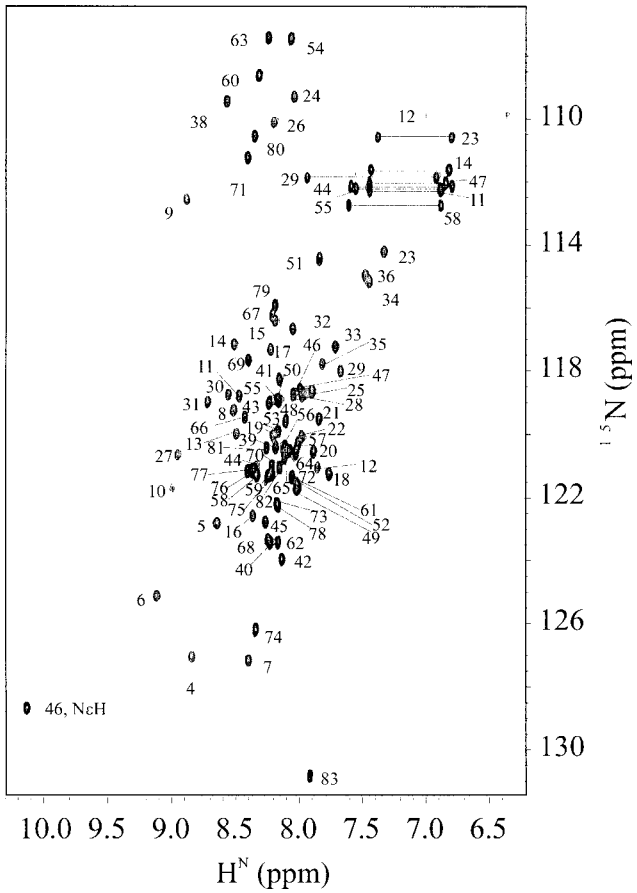

Figure 2 2D ^{1}H-^{15}N-HSQC spectrum of ParD

The spectrum of 0.6 mM ParD in 90% buffer (20 mM phosphate, pH 6.0/50 mM KCl) and 10% $^{2}H_2O$ is shown with ^{15}N-^{1}H resonance assignments.

ambiguously (Figure 2). The dimeric form is symmetrical, because only one set of signals was observed. The N-terminal residue Arg^3 could not be found in the ^{15}N-edited spectra but was observed in ^{13}C-edited spectra. For the other nuclei the percentage of assignment was 98% for Cα and 97% for Cβ and C′. The side-chain assignment was also essentially complete where the missing resonances could be attributed mainly to the less well-ordered C-terminal part of the protein. A table of the chemical shifts assigned has been deposited in the BioMagRes data bank (http://www.bmrb.wisc.edu) under the accession number 4792.

The secondary-structure assignment of ParD is based on the consensus chemical-shift index (CSI) method, including $^{13}C\alpha$, $^{13}C\beta$, $^{13}C'$ and Hα shifts [30]. These data show very clearly the formation of a β-strand in the N-terminal region (Leu^4–Thr^9) followed by α-helical stretches that are interrupted by short loop regions (Figure 3). The first three α-helical regions were well defined in the CSI data, reaching from Gln^{11} to Ala^{21}, Lys^{28} to Leu^{35} and Ala^{40} to Leu^{49}, respectively, which make 35% of the α-helical regions and 7% of the β-sheet content. Consensus chemical shifts and NOE data (Figures 3B and 3C) indicate that the C-terminal region is less well ordered or undergoing rapid conformational change on the NMR timescale. However, $^{13}C\alpha$ chemical shifts show a tendency for the formation of further α-helices beyond the well-ordered N-terminal domain.

Unambiguous $^{3}J_{\alpha H\text{-}NH}$ coupling constants characteristic of β-structures were derived for the residues Leu^4, Thr^5 and Met^8; small coupling constants characteristic of α-helices were found clustered in the three α-helical regions of ParD (Figure 3B). These data are in good agreement with the predicted secondary structure (Figure 3A) reporting an N-terminal β-ribbon (Arg^3–Ile^6) followed by α-helical stretches (Asp^{10} to Gln^{23}, Ile^{27} to Leu^{35}, Ala^{42} to Arg^{56} and Val^{70} to Leu^{78}), which correspond to 57% of the α-helices and 5% of the extended structure. Protein-fold-recognition database searches [28] using only residues Met^1–Lys^{50} found a match with CopG protein, a known member of the ribbon-helix-helix family.

The β-ribbon was formed by a typical alternating hydrophobic–hydrophilic pattern of amino acids (Leu^4-Thr-Ile-Asp-

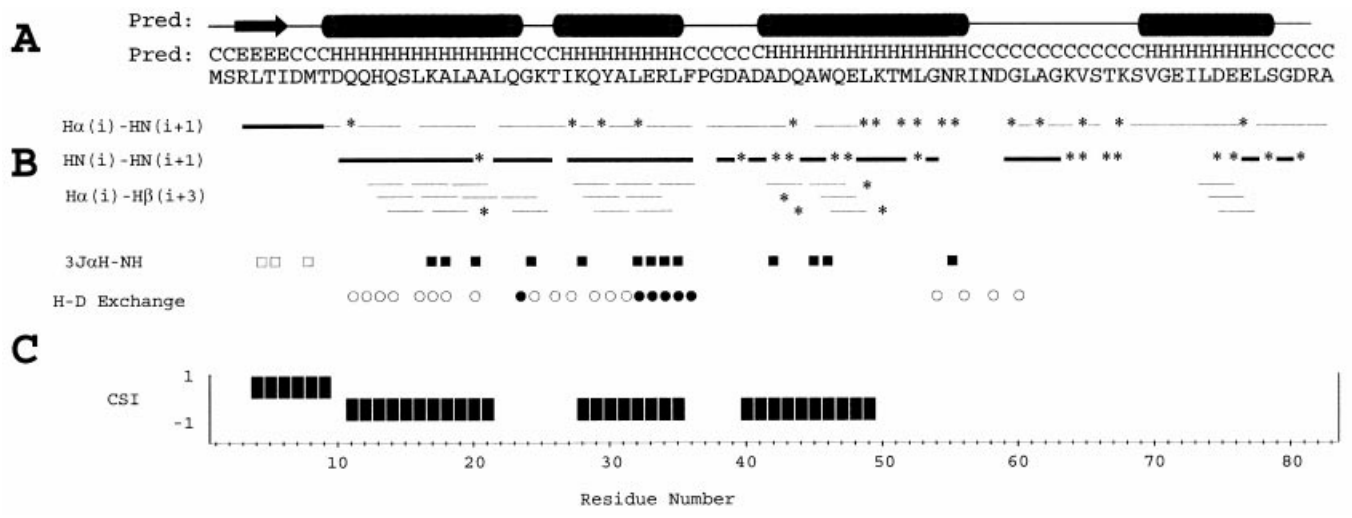

Figure 3 Summary of the structural information about ParD obtained from NMR

(**A**) The amino acid sequence of ParD and its predicted (Pred) secondary structure [27]. The arrow represents the β-strand region and bars represent α-helical regions. (**B**) Observed short-range NOEs typical of α-helices and β-structures are depicted, with line thickness representing the strength of NOEs; NH–NH resonances that were indistinguishable due to overlapping signals are tagged with *. The amide signals present 45 min after dissolving the lyophilized protein in ^2H_2O are represented by ○, whereas ● represents exchanging amides still present after 2 h. Large ($>$ 7 Hz) and small ($<$ 5 Hz) $^3J_{\alpha H\text{-}NH}$ coupling constants typical for extended and helical structural elements are represented by □ and ■, respectively. (**C**) The extracted data from chemical-shift analysis with the consensus CSI data displayed in the bottom row.

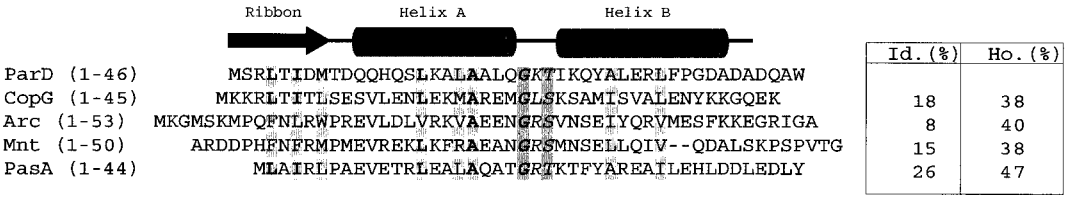

Id. (%)	Ho. (%)
18	38
8	40
15	38
26	47

Figure 4 Alignment of ParD (Met^1–Trp^{46}) with the ribbon-helix-helix proteins CopG, Arc and Mnt and the closest antidote relative PasA

The secondary-structure diagram was derived from the 3D structure of CopG protein. Conserved residues are depicted in bold, conserved hydrophobic residues are shaded in light grey, other conserved residues are shaded in dark grey. The highly conserved turn connecting helices A and B is shown in italics. Sequence identities (Id) and homologies (Ho) of the pairwise alignments of the respective proteins with ParD are listed.

Met-Thr^9). Further hydrophobic residues at conserved positions were Leu^{16}, Leu^{19}, Ala^{20}, Ala^{31} and Leu^{35}. These corresponded to Leu^{17}, Met^{20}, Ala^{21}, Leu^{32} and Leu^{36} in CopG, Val^{22}, Val^{25}, Ala^{26}, Ile^{37} and Val^{41} in Arc and Leu^{19}, Val^{22}, Ala^{23}, Leu^{34} and Val^{38} in Mnt (Figure 4). From the known 3D structures of Arc, Mnt and CopG [20,31–33], it can be seen clearly that these residues are important for forming the hydrophobic core of this folding motif. The turn between the first and second helices starts in all cases with a glycine residue displaying the typical GXT/S pattern (Figure 4). The N-terminal part of PasA (Met^1–Tyr^{44}) fits nicely into this pattern of conserved hydrophobic residues, as demonstrated in Figure 4. After a gap of 5 amino acids corresponding to Gln^{47}–Thr^{51} in ParD, the C-terminal sequence aligns well with ParD. The sequence identity/homology between PasA and ParD were 27/50% for the N-terminal domain (Arg^3–Trp^{46}) and 26/47% for the whole sequence, respectively. These values differ slightly from the ones published previously [25] due to minor deviations in alignment. Identities and homologies between ParD and members of the ribbon-helix-helix family were calculated and showed surprisingly low sequence identities but high homologies (Figure 4).

Amide hydrogen-exchange data indicated that the most protected area ranged from Leu^{32} to Phe^{36}, which resides within the cluster of slowly exchanging amides covering most of helices A and B. This region, together with the hydrophobic residues of the β-ribbon, forms the central core and the dimerization interface of the protein.

To characterize the dynamic properties of ParD, relaxation measurements were performed with ^{15}N-labelled protein. Heteronuclear NOEs sensitive to rapid internal motions were calculated from the ratio of the peak heights in the spectra acquired with and without ^{1}H saturation. The missing resonances (Ser^{15}, Leu^{19}, Met^{52}, Asn^{55}, Arg^{56}, Asn^{58}, Asp^{59} and Glu^{72} for T_1, Asp^{44}, Ala^{45}, Gln^{47} and Leu^{53} for T_2 plus Ile^{57}, Leu^{61} and Ile^{73} for the heteronuclear NOE) could not be obtained reliably owing to spectral overlap (Figure 5). The negative NOE values for the C-terminal domain (Asp^{59}–Ala^{83}) indicate the presence of significant flexibility in this region. This is in excellent agreement with the ^{15}N-T_1 and ^{15}N-T_2 relaxation times, which clearly show two structurally different moieties ranging from Leu^4 to Ile^{57} for the well-structured N-terminus and from Asn^{58} to Ala^{83} for the remaining flexible C-terminal region. Cα chemical-shift data

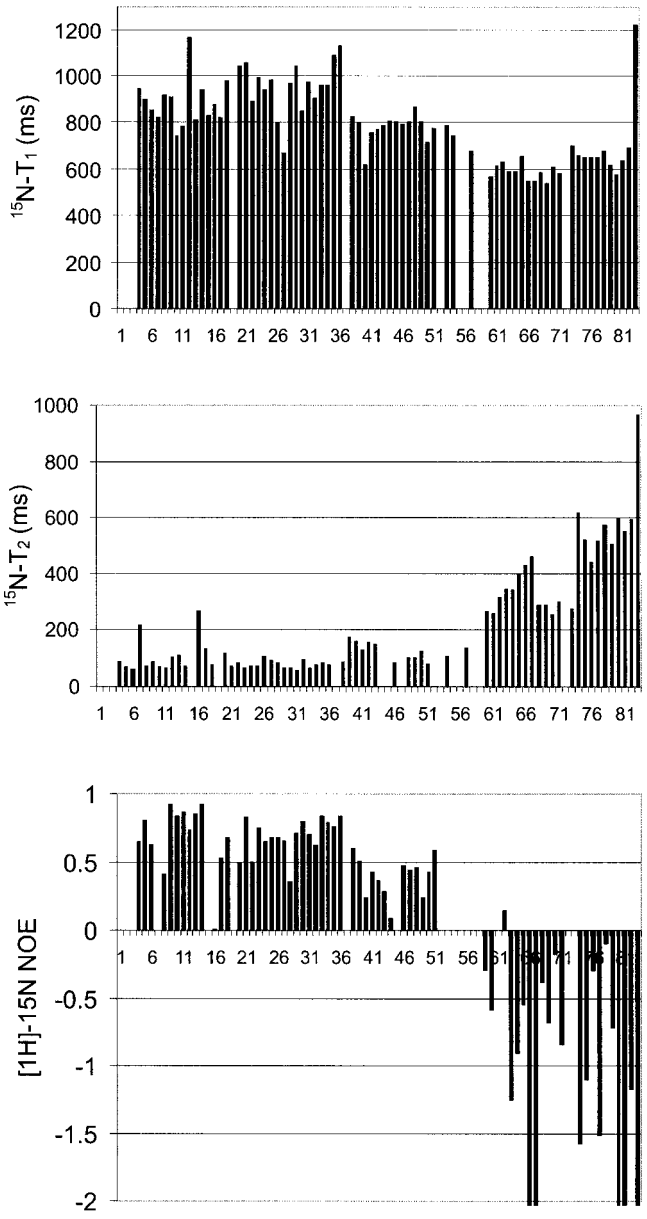

Figure 5 Relaxation data for the ^{15}N nuclei of ParD

^{15}N-T$_1$, ^{15}N-T$_2$ and [^{1}H]-^{15}N-heteronuclear NOE data are plotted as a function of residue number.

show a down-field shift from the random-coil values for residues in the C-terminus for residues 58–64, 66, 68–72, 74–81 and 83, indicating a tendency for the formation of helical structures. The deviations are, however, smaller than in the N-terminal region, which again supports the presence of a predominantly unstructured C-terminal domain. As the C-terminal fragment of ParD appears to be responsible for ParE binding [17], we expect this domain to become ordered upon anti-toxin–toxin complex formation.

TFE-induced secondary-structure changes

TFE was added to a ParD solution and changes in the secondary structure were monitored by CD spectroscopy. Upon an increase in the TFE concentration (from 0 to 5, 10, 20, 30, 40, 50, 60, 70 and 80%) the α-helical content rose gradually (from 37

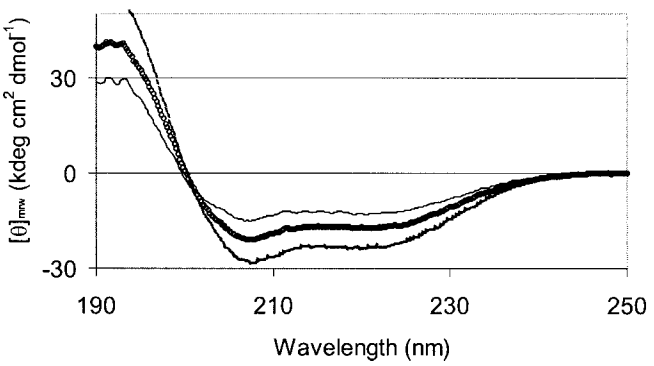

Figure 6 Effect of the hydrophobic agent TFE

The far-UV CD spectra of ParD (23 μM) in 20 mM potassium phosphate buffer, pH 7.5/20 mM KCl, incubated with increasing amounts of TFE (0%, thin line; 20%, ○; 80%, thick line), were monitored.

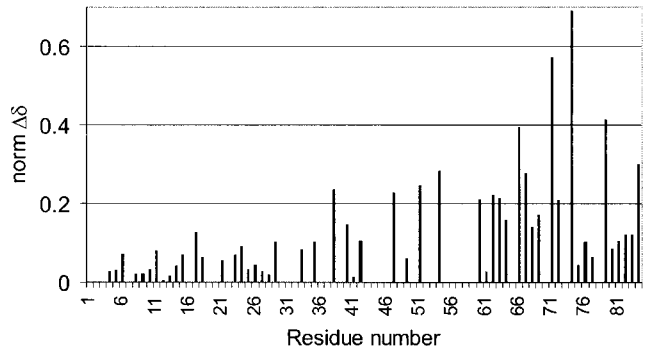

Figure 7 Titration of ParD with TFE

The chemical-shift differences in the resonances observed in ^{1}H-^{15}N-HSQC spectra between ParD in phosphate buffer and ParD in buffer plus 15% TFE are plotted against residue number. Missing bars are either due to spectral overlap or ambiguous shifts after titration.

to 44, 50, 53, 55, 62, 65, 68, 70 and 72%) with an isodichroic point at 200.4 nm (Figure 6). The same titration was investigated using NMR spectroscopy. With increasing TFE concentrations the amide proton line widths were broadened in the acquired 2D ^{1}H-^{15}N-HSQC spectra and led to high spectral overlap, thus preventing a more detailed study of the dynamic behaviour (results not shown). As can be seen from the combined chemical-shift changes (Figure 7), addition of TFE influenced mainly the residues starting from Gly^{38}, resulting in major chemical-shift differences. This indicates a transition from the more flexible and random-coil C-terminal moiety to an α-helical domain consistent with the CD experiment.

DISCUSSION

The secondary-structure assignment based on the CSI and sequential NOEs clearly shows the existence of a short N-terminal β-sheet followed by three α-helices. The overall secondary-structure content, as estimated from the consensus CSI, matched those data determined by CD spectroscopy, namely 37% α-helical regions and 12% β-structure [8]. The small discrepancy in β-content arises from the difficulty in getting accurate estimates of the β-structure by CD spectroscopy due to the less-pronounced contributions of β-structures compared with the α-helical signal.

Secondary-structure prediction yields a significantly higher α-helical content (57%), which results from an additional helix (Figure 3A). Experimental $^{13}C\alpha$ chemical-shift data, however, only indicate a propensity for α-helical regions in the C-terminus.

We tried to induce this 'missing' helicity by the addition of TFE, which is known to stabilize helical structures but also to disrupt native tertiary structure by modifying non-local hydrophobic interactions in polypeptides and proteins [34–36]. The structural changes of ParD, which are induced by TFE addition as observed in the near-UV CD spectrum, indicate the formation of additional helical structure. As monitored by NMR spectroscopy, C-terminal residues appear to be involved mainly in these changes. However, due to extensive line-broadening and resulting overlaps the NMR data were only interpretable up to a TFE concentration of 15%. Therefore a more detailed assignment of the TFE-induced changes to particular regions of the polypeptide chain could not be carried out.

ParD protein can be aligned with CopG and Arc, which belong to a family of small prokaryotic repressors displaying a homodimeric ribbon-helix-helix fold in their 3D structures. This distribution of secondary-structural elements is corroborated by our experimental data derived from NMR solution studies (Figure 3).

It has been hypothesized previously that ParD might belong to this fold family [37], despite lack of experimental evidence and the low sequence homology between ParD and the mentioned repressor proteins. On the basis of the alignment of secondary-structure elements and the pattern of hydrophobic residues it is now evident that ParD belongs to the ribbon-helix-helix fold family and that the mode of DNA binding is analogous to that seen in the crystal structures of the DNA complexes of Arc [31], MetJ [38] and CopG [20]. Therefore we expect the short intermolecular β-ribbon to insert into the major groove of the DNA at the specific binding site.

Secondary-structure predictions for the antidotes Phd, CcdA, PemI [39], RelB and PasA (results not shown) suggest the presence of a β-ribbon followed by α-helices. In analogy, antidote proteins of these functional homologous addiction systems most probably belong to this fold family as well, even though the systems are only related weakly at the protein-sequence level. Homology has been reported for *ccdA* and *pemI* [40] as well as for *mazE* (*chpAI*) [41], and within the large family of *relBE* systems [14]. Amongst all the characterized antidote proteins, the closest related to ParD is PasA from the Gram-negative acidophilic bacterium *Thiobacillus ferrooxidans* [25]. The complete amino acid sequence of PasA (74 residues) can be aligned with that of ParD and, consequently, the ribbon-helix-helix motif is proposed for the N-terminal domain (Figure 4).

The relaxation measurements together with the chemical-shift data indicate clearly that the ParD protein is divided into two domains: a well-ordered N-terminal domain containing the $\beta\alpha\alpha$ secondary-structure elements and a very flexible C-terminal domain.

These data are in excellent agreement with the two biological roles of ParD, namely its repressor and antidote functions, and with biochemical data showing that the DNA-binding function resides in the N-terminal part of the protein while the toxin-binding activity is suggested to reside in the C-terminal part [17]. Similar to the conformational changes reported of the CcdA/CcdB and PhD/Doc modules upon complex formation [42,43], we expect the C-terminal part of ParD to acquire a higher degree of order upon binding to the ParE protein.

The availability of an increasing number of complete genomes has revealed the presence of addiction systems on many chromosomes of Gram-positive and Gram-negative bacteria as well as the Archaea. Although their function has not been elucidated they are bound to convey some evolutionary advantage to the host. The low sequence homology between antidotes of the diverse addiction systems may reflect the necessity to develop a high specificity (for DNA and target binding) in order to be useful to the host organism.

We thank Don Helinski for expression strains, Robert Konrat and Heinz Sterk for fruitful discussions, and Edith Kraner for help with preparation of the manuscript. This work was supported by the Fonds zur Förderung der Wissenschaftlichen Forschung (grant no. P12559-GEN). K.Z. thanks the Austrian Academy of Sciences for an APART Fellowship.

REFERENCES

1 Jensen, R. B. and Gerdes, K. (1995) Programmed cell death in bacteria: proteic plasmid stabilization systems. Mol. Microbiol. **17**, 205–210
2 Holcik, M. and Iyer, V. N. (1997) Conditionally lethal genes associated with bacterial plasmids. Microbiology **143**, 3403–3416
3 Engelberg-Kulka, H. and Glaser, G. (1999) Addiction modules and programmed cell death and antideath in bacterial cultures. Annu. Rev. Microbiol. **53**, 43–70
4 Rawlings, D. E. (1999) Proteic toxin-antitoxin, bacterial plasmid addiction systems and their evolution with special reference to the pas system of pTF-FC2. FEMS Microbiol. Lett. **176**, 269–277
5 Cooper, T. F. and Heinemann, J. A. (2000) Postsegregational killing does not increase plasmid stability but acts to mediate the exclusion of competing plasmids. Proc. Natl. Acad. Sci. U.S.A. **97**, 12643–12648
6 Gerdes, K. (2000) Toxin-antitoxin modules may regulate synthesis of macromolecules during nutritional stress. J. Bacteriol. **182**, 561–572
7 Jensen, R. B., Grohmann, E., Schwab, H., Diaz Orejas, R. and Gerdes, K. (1995) Comparison of ccd of F, parDE of RP4, and parD of R1 using a novel conditional replication control system of plasmid R1. Mol. Microbiol. **17**, 211–220
8 Oberer, M., Lindner, H., Glatter, O., Kratky, C. and Keller, W. (1999) Thermodynamic properties and DNA binding of the ParD protein from the broad host-range plasmid RK2/RP4 killing system. Biol. Chem. **380**, 1413–1420
9 Johnson, E. P., Strom, A. R. and Helinski, D. R. (1996) Plasmid RK2 toxin protein ParE: purification and interaction with the ParD antitoxin protein. J. Bacteriol. **178**, 1420–1429
10 Dao-Thi, M. H., Messens, J., Wyns, L. and Backmann, J. (2000) The thermodynamic stability of the proteins of the ccd plasmid addiction system. J. Mol. Biol. **299**, 1373–1386
11 Santos Sierra, S., Giraldo, R. and Diaz Orejas, R. (1998) Functional interactions between chpB and parD, two homologous conditional killer systems found in the *Escherichia coli* chromosome and in plasmid R1. FEMS Microbiol. Lett. **168**, 51–58
12 Gazit, E. and Sauer, R. T. (1999) Stability and DNA binding of the phd protein of the phage P1 plasmid addiction system. J. Biol. Chem. **274**, 2652–2657
13 Le Dantec, C., Winter, N., Gicquel, B., Vincent, V. and Picardeau, M. (2001) Genomic sequence and transcriptional analysis of a 23-kilobase mycobacterial linear plasmid: evidence for horizontal transfer and identification of plasmid maintenance systems. J. Bacteriol. **183**, 2157–2164
14 Gronlund, H. and Gerdes, K. (1999) Toxin-antitoxin systems homologous with relBE of *Escherichia coli* plasmid P307 are ubiquitous in prokaryotes. J. Mol. Biol. **285**, 1401–1415
15 Heidelberg, J. F., Eisen, J. A., Nelson, W. C., Clayton, R. A., Gwinn, M. L., Dodson, R. J., Haft, D. H., Hickey, E. K., Peterson, J. D., Umayam, L. et al. (2000) DNA sequence of both chromosomes of the cholera pathogen *Vibrio cholerae*. Nature (London) **406**, 477–483
16 Simpson, A. J., Reinach, F. C., Arruda, P., Abreu, F. A., Acencio, M., Alvarenga, R., Alves, L. M., Araya, J. E., Baia, G. S., Baptista, C. S. et al. (2000) The genome sequence of the plant pathogen *Xylella fastidiosa*. The *Xylella fastidiosa* Consortium of the Organization for Nucleotide Sequencing and Analysis. Nature (London) **406**, 151–157
17 Roberts, R. C., Spangler, C. and Helinski, D. R. (1993) Characteristics and significance of DNA binding activity of plasmid stabilization protein ParD from the broad host-range plasmid RK2. J. Biol. Chem. **268**, 27109–27117
18 Salmon, M. A., Van Melderen, L., Bernard, P. and Couturier, M. (1994) The antidote and autoregulatory functions of the F plasmid CcdA protein: a genetic and biochemical survey. Mol. Gen. Genet. **244**, 530–538
19 Phillips, S. E. (1994) The beta-ribbon DNA recognition motif. Annu. Rev. Biophys. Biomol. Struct. **23**, 671–701
20 Gomis-Ruth, F. X., Sola, M., Acebo, P., Parraga, A., Guasch, A., Eritja, R., Gonzalez, A., Espinosa, M., del Solar, G. and Coll, M. (1998) The structure of plasmid-encoded transcriptional repressor CopG unliganded and bound to its operator. EMBO J. **17**, 7404–7415

21 Cavanagh, J., Fairbrother, W. J. and Palmer, A. G. (1995) Protein NMR Spectroscopy: Principles and Practice, Academic Press, London

22 Delaglio, F., Grzesiek, S., Vuister, G. W., Zhu, G., Pfeifer, J. and Bax, A. (1995) NMRPipe: a multidimensional spectral processing system based on UNIX pipes. J. Biomol. NMR **6**, 277–293

23 Bartels, C., Xia, T.-H., Billeter, M., Güntert, P. and Wüthrich, K. (1995) The program XEASY for computer-supported NMR spectral analysis of biological macromolecules. J. Biomol. NMR **5**, 1–10

24 Johnson, B. A. and Blevins, R. A. (1994) NMRView: a computer program for the visualization and analysis of NMR data. J. Biomol. NMR **4**, 603–614

25 Smith, A. S. and Rawlings, D. E. (1997) The poison-antidote stability system of the broad-host-range *Thiobacillus ferrooxidans* plasmid pTF-FC2. Mol. Microbiol. **26**, 961–970

26 Thompson, J. D., Higgins, D. G. and Gibson, T. J. (1994) CLUSTAL W: improving the sensitivity of progressive multiple sequence alignment through sequence weighting, position-specific gap penalties and weight matrix choice. Nucleic Acids Res. **22**, 4673–4680

27 Jones, D. T. (1999) Protein secondary structure prediction based on position-specific scoring matrices. J. Mol. Biol. **292**, 195–202

28 Jones, D. T. (1999) GenTHREADER: an efficient and reliable protein fold recognition method for genomic sequences. J. Mol. Biol. **287**, 797–815

29 Berman, H. M., Westbrook, J., Feng, Z., Gilliland, G., Bhat, T. N., Weissig, H., Shindyalov, I. N. and Bourne, P. E. (2000) The Protein Data Bank. Nucleic Acids Res. **28**, 235–242

30 Wishart, D. and Sykes, B. (1994) The ^{13}C chemical-shift index: a simple method for the identification of protein secondary structure using ^{13}C chemical-shift data. J. Biomol. NMR **4**, 171–180

31 Raumann, B. E., Rould, M. A., Pabo, C. O. and Sauer, R. T. (1994) DNA recognition by beta-sheets in the Arc repressor-operator crystal structure. Nature (London) **367**, 754–757

32 Burgering, M. J., Boelens, R., Gilbert, D. E., Breg, J. N., Knight, K. L., Sauer, R. T. and Kaptein, R. (1994) Solution structure of dimeric Mnt repressor (1-76). Biochemistry **33**, 15036–15045

Received 9 July 2001/10 October 2001; accepted 25 October 2001

33 Nooren, I. M., Rietveld, A. W., Melacini, G., Sauer, R. T., Kaptein, R. and Boelens, R. (1999) The solution structure and dynamics of an Arc repressor mutant reveal premelting conformational changes related to DNA binding. Biochemistry **38**, 6035–6042

34 Jasanoff, A. and Fersht, A. R. (1994) Quantitative determination of helical propensities from trifluoroethanol titration curves. Biochemistry **33**, 2129–2135

35 Buck, M., Radford, S. E. and Dobson, C. M. (1993) A partially folded state of hen egg white lysozyme in trifluoroethanol: structural characterization and implications for protein folding. Biochemistry **32**, 669–678

36 Gast, K., Zirwer, D., Muller-Frohne, M. and Damaschun, G. (1999) Trifluoroethanol-induced conformational transitions of proteins: insights gained from the differences between alpha-lactalbumin and ribonuclease A. Protein Sci. **8**, 625–634

37 Eberl, L., Givskov, M. and Schwab, H. (1992) The divergent promoters mediating transcription of the par locus of plasmid RP4 are subject to autoregulation. Mol. Microbiol. **6**, 1969–1979

38 Somers, W. S. and Phillips, S. E. (1992) Crystal structure of the met repressor-operator complex at 2.8 A resolution reveals DNA recognition by beta-strands. Nature (London) **359**, 387–393

39 Magnuson, R., Lehnherr, H., Mukhopadhyay, G. and Yarmolinsky, M. B. (1996) Autoregulation of the plasmid addiction operon of bacteriophage P1. J. Biol. Chem. **271**, 18705–18710

40 Ruiz Echevarria, M. J., de Torrontegui, G., Gimenez Gallego, G. and Diaz Orejas, R. (1991) Structural and functional comparison between the stability systems ParD of plasmid R1 and Ccd of plasmid F. Mol. Gen. Genet. **225**, 355–362

41 Masuda, Y., Miyakawa, K., Nishimura, Y. and Ohtsubo, E. (1993) chpA and chpB, *Escherichia coli* chromosomal homologs of the pem locus responsible for stable maintenance of plasmid R100. J. Bacteriol. **175**, 6850–6856

42 Van Melderen, L., Thi, M. H. D., Lecchi, P., Gottesman, S., Couturier, M. and Maurizi, M. R. (1996) ATP-dependent degradation of CcdA by Lon protease. Effects of secondary structure and heterologous subunit interactions. J. Biol. Chem. **271**, 27730–27738

43 Gazit, E. and Sauer, R. T. (1999) The Doc toxin and Phd antidote proteins of the bacteriophage P1 plasmid addiction system form a heterotrimeric complex. J. Biol. Chem. **274**, 16813–16818